Tel-Cu-NPs Catalyst: Synthesis of Naphtho[2,3-*g*]phthalazine Derivatives as Potential Inhibiters of Tyrosinase Enzymes and Their Investigation in Kinetic, Molecular Docking, and Cytotoxicity Studies

Keerthana Selvaraj [1], **Ali Daoud** [2] , **Saud Alarifi** [2] **and Akbar Idhayadhulla** [1,*]

[1] Research Department of Chemistry, Nehru Memorial College (Affiliated to Bharathidasan University), Puthanampatti 621007, Tamil Nadu, India; keerthraj.akfarm@gmail.com

[2] Department of Zoology, College of Sciences, King Saud University (KSU), P.O. Box 2455, Riyadh 11451, Saudi Arabia; aalidaoud@ksu.edu.sa (A.D.); salarifi@ksu.edu.sa (S.A.)

* Correspondence: idhayadhulla@nmc.ac.in

Abstract: Novel one-pot synthesis naphtho[2,3-g]phthalazine (**1a–1k**) of Mannich base derivatives can be achieved via grindstone chemistry using a Tel-Cu-NPs (telmisartan-copper nanoparticles) catalyst. This method offers efficient mild reaction conditions and high yields. Tyrosinase inhibitory activity was evaluated for all synthesized compounds, along with analysis of kinetic behavior and molecular docking studies. The synthesized compound, **1c** was (IC$_{50}$ = 11.5 μM) more active than kojic acid (IC$_{50}$ = 78.0 μM). Lineweaver Burk plots were used to analyze the kinetic behavior of the most active compound **1c**, it was reversible and competitive behavior. Compound **1c** and kojic acid occurred in the presence of 2-hydroxyketone, which has the same inhibitory mechanism. The molecular docking of compound **1c** and the control kojic acid were docked against 2Y9X protein via the Schrodinger Suite. The compound **1c** showed a respectable dock score (−5.6 kcal/mol) compared to kojic acid with a dock score of (−5.2 kcal/mol) in the 2Y9X protein. Cytotoxicity activity was also evaluated by using HepG2 (liver), MCF-7 (breast), and HeLa (cervical) cancer cell lines, and high activity for **1c** (GI$_{50}$ = 0.01, 0.03, and 0.04 μM, respectively) against all cell lines was found compared to standard and other compounds. Therefore, this study succeeded in testing a few promising molecules as potential antityrosinase agents.

Keywords: Tel-Cu-Nps catalyst; naphtho[2,3-g]phthalazine; kojic acid; mushroom tyrosinase; molecular docking; kinetic behaviour; cytotoxicity activity

1. Introduction

Out of several green chemistry methodologies, one simple and rapid methodology to prepare chemical and pharmaceutical compounds is via grindstone chemistry. This method was developed by Toda et al., who showed that many, but not all, reactions can be carried out by just grinding or triturating the solids together [1]. The Mannich reaction, which is a popular reaction in organic and medicinal chemistry domains [2], is a condensation reaction that forms an imminium-ion by enol-forming a carbonyl compound. The presently known Mannich type reactions face significant challenges. One of the prime challenges is the reaction time. Other challenges include harsh reaction conditions, toxicity, catalyst requirements, and the tedious methods required to separate and purify the final product(s). Some of the proposed methodologies to address these challenges include synthetic methodologies; for example,

the use of Lewis acids or bases, ultrasound irradiation, or microwave, or the use of solubilizing agents or surfactant-type catalysts to address the insolubility of most organic compounds in water [3]. In addition, some of the known green trends in the Mannich reaction include ball-milling solvent-free [4], or with ionic liquid medium [5], nanoparticles [6], or enzymes in bio-catalytic conditions [7,8]. These green trends in the Mannich reaction also suffer with the challenges outlined above. Tyrosinase is a copper-containing mixed-function oxidase which is usually scattered in microorganisms, plants, and animals. Tyrosinase transforms into dopaquinone, which signifies the first step of melanin biosynthesis. o-quinones can polymerize naturally to melanin pigments [9]. o-diphenols are converted to o-quinones [10], which are involved in melanin synthesis in two separate reactions, and melanin is a biopolymer that is responsible for pigmentation [11]. However, the pigmentation can cause some dermatological disorders [12]. Tyrosinase is linked to neurodegeneration diseases associated with the creation of dopaquinone by oxidation of dopamine, which results in neuronal damage and cell death [13]. As a result, the medical, agricultural, and cosmetic industries are looking for effective tyrosinase inhibitors with minimal side effects. Derivatives of 9,10-anthraquinone have displayed various pharmacological effects, including laxative [14], anticancer [15], anti-inflammatory [16], antiarthritic [17], antifungal [18], antibacterial [19], antiviral [20], antiplatelet [21], and neuroprotective effects [22]. In addition, anthraquinone and its analogues have excellent properties, such as high excitation, emission, and absorption coefficients within the visible wavelength region, and low toxicity [23,24]. Some researchers have reported that benzo[g]phthalazines have the ability to form dinuclear complexes with Cu(II) when assayed with 1,4-bis(alkylamino)benzo[g]phthalazines. However, there has been no research focused on naphtho[g]phthalazine synthesis and biological screening [25]. This study focused on naphtho[2,3-g]phthalazine models covered by anthraquinone analogues in order to analyze the effect of antityrosinase activity.

Based on the above observations, the tyrosinase inhibitory activities of naphtho[2,3-g]phthalazine derivatives have not been previously studied. In this study, we designed new compounds bearing a carbonyl and hydroxyl group on the naphtho[2,3-g]phthalazine ring (Figure 1). Thus, we studied a new naphtho[2,3-g]phthalazine core belonging to the group of anthraquinone derivatives, and evaluated their anti-tyrosinase activity in vitro. Our kinetic studies also allowed us to discuss and compare molecular docking results compared with wet lab results.
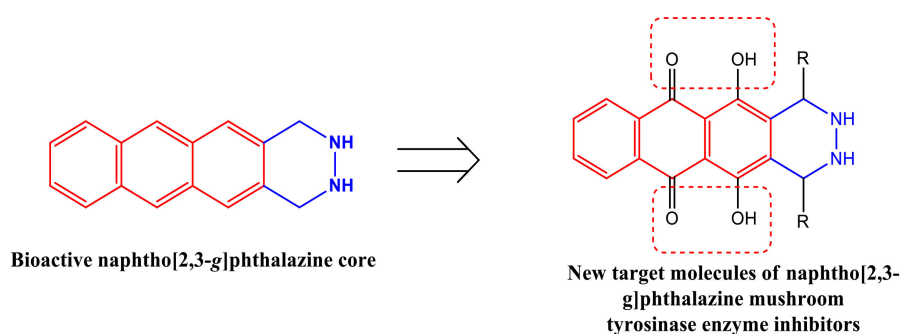

**Figure 1.** Target molecules of tyrosinase enzyme inhibitors.

2. Results and Discussion

2.1. Chemistry

2.1.1. Synthesis of Catalysis

Scheme 1 shows the route of preparation of telmisartan nanoparticles (Tel-Cu-NPs). First, the CuCl$_2$·2H$_2$O was mixed with telmisartan in ethanol with grinding for up to 10 min. A light blue solid material was obtained, and this solid material was mixed with 1 M NaOH and maintained at pH = 7. The obtained solid material was converted into a sky blue precipitate, followed by addition

of water. The final solid material was filtered and purified with suitable techniques. The synthesized Cu-NPs were confirmed by XRD, SEM, and EDX analysis.
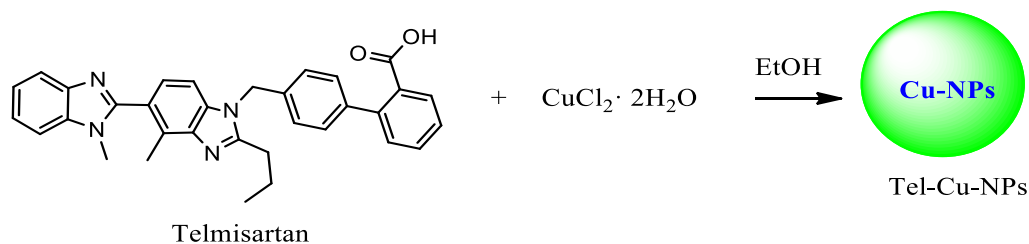
Scheme 1. Synthesis of Tel-Cu-NPs (telmisartan-copper nanoparticles).

2.1.2. Powder X-Ray Diffraction Studies

The structural analysis and phase crystallinity of the synthesized Cu-NPs were examined via the powder X-ray diffraction method. Figure 2 shows the Cu nanoparticle diffraction pattern at a 2θ value of 43.20°, 50.42°, and 74.15° with respect to the (111), (200), and (220) planes individually. A copper cubic lattice formation can be seen. JCPDS No. 040836 indicates that there was good agreement compared with the standard pattern for a pure face centered cubic of Cu-NPs. There were no impurity peaks. From the observed main diffracted peak, the average crystalline size could be calculated using the Scherer equation:

$$D_{(hkl)} = \frac{k\lambda}{\beta \cos \theta}, \tag{1}$$

where $D_{(hkl)}$ is the size, k is the shape constant (0.89), λ is the incident X-ray (Cu $k\alpha$ source, $\lambda = 0.15405$ nm), β is the full width at half-maximum, and θ is the incident angle of the X-ray. The average crystallite size of the synthesized copper nanoparticles was 25.41 nm.
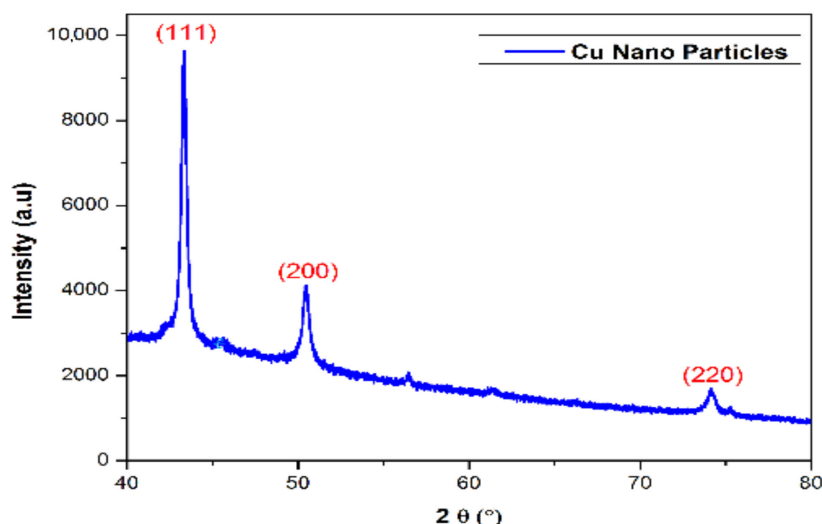

Figure 2. XRD Studies of telmisartan mediated copper nanoparticle.

2.1.3. SEM and EDX Analysis

Figure 3 shows the morphology of the SEM images of the Cu-NPs obtained in water. A 200 nm particle size was found, conforming to the formation of Cu nanoparticles from telmisartan. Figure 4 shows the EDX of Cu-NPs that exhibited the elements Cu, C, and O in the nanoparticles, conformed by the formation of the nanoparticle.
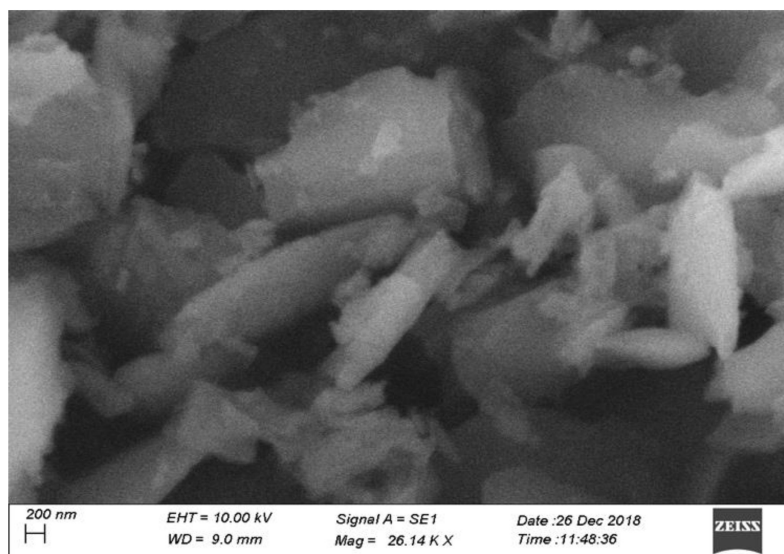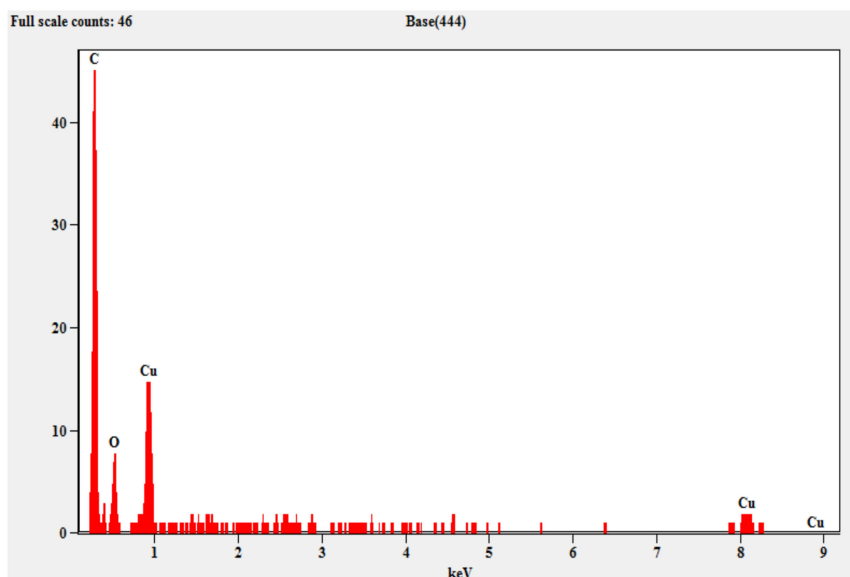
Figure 3. Telmisartan Cu-NPs of SEM images.

Figure 4. Telmisartan-copper nanoparticle of EDX.

Naphtho[2,3-g]phthalazine (**1a**–**1k**) was synthesized as shown in Scheme 2. First, the 1,4-dihydroxy-anthraquinone of 1 with aldehyde (2.1 equiv.) in the presence of hydrazine hydrate (1.0 equiv.) and Tel-Cu-NPs catalysis in EtOH at RT gave naphtho[2,3-g]phthalazine with a 95% yield. Compounds of **1a**–**1k** were purified by column chromatography, and their structure was determined by spectroscopic analysis. Assignment of the selected characteristic IR bands of compounds **1a**–**1k** exposed the functional groups OH, NH, and C=O, which obtained strong absorption band ranges between 3406–3414 cm^{-1}, 3280–3286 cm^{-1}, and 1750–1754 cm^{-1}, respectively. The ^{1}H-NMR spectra show signals at δ 5.30–5.39 and 9.20–9.86 ppm corresponding to the OH and NH protons, respectively. The ^{13}C NMR spectrum shows signals from δ 187.1–187.6, 151.5–153.9, and 50.7–60.8 ppm, that correspond to the C=O, -C-OH, and -C-N carbon atoms individually. In addition, mass spectra show that all compounds of molecular weight conformed to molecular ion peaks present in the mass spectral analysis.
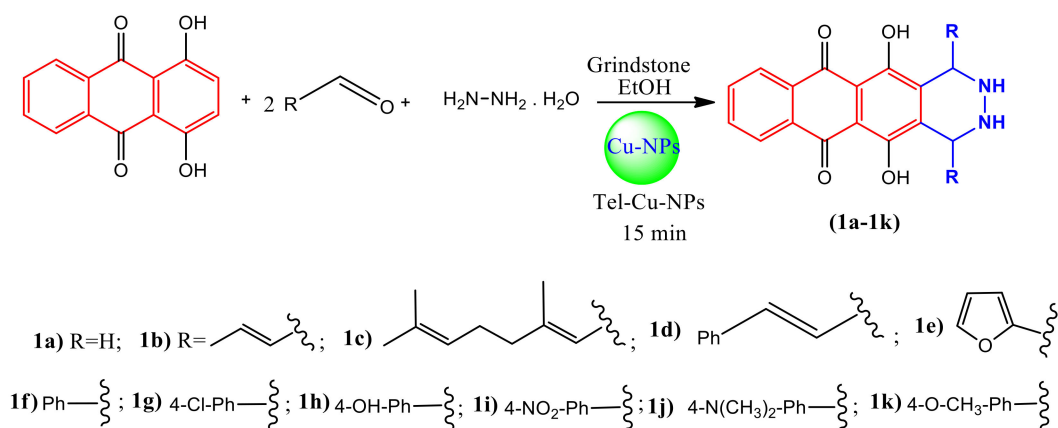
Scheme 2. Synthesis of target compounds (**1a–1k**).

2.1.4. Catalyst Recovery Studies

Figure 5 shows the recovery of the catalyst salvaged from at least 10 run times, with a slight loss in catalytic activity. The lessening of activity could be detected with the regenerated catalyst on salvaging due to the surface area of the catalyst during the reaction, or partial loss of the basic sites/regeneration. The application of the catalyst was inspected by optimizing the reaction conditions. A number of aldehydes were selected for the condensation reaction with the Cu-NPs (1 mole %) catalyst at room temperature in a solvent-free setting, and the yield is reported in Table 1. The Cu-catalyzed performance and reaction mechanism are shown in Scheme 3.
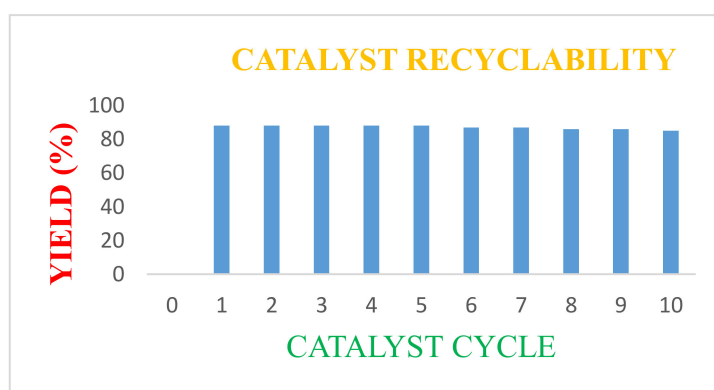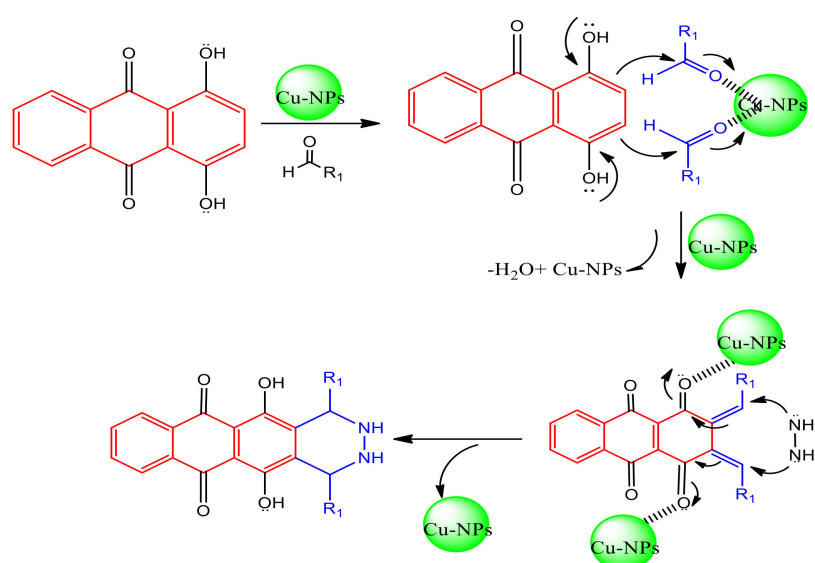

Figure 5. Recyclability of telmisartan mediated copper nanoparticle.

Table 1. Catalyst recyclability.

Entry	Catalyst Use	Yield (%)
1	1st	86
2	2nd	85
3	3rd	84
4	4th	84
5	5th	83
6	6th	81
7	7th	84
8	8th	82
9	9th	81
10	10th	81

Scheme 3. Mechanism of reaction compound (**1a–1k**).

2.2. Biological Activity

2.2.1. Antityrosinase Activity

Inhibition of naphtho[2,3-g]phthalazine was tested using 3,4-dihydroxy-L-phenylalanine (L-DOPA) as the substrate. Kojic acid was used as one of the basic skin whitening elements, as a reference compound for this study. Table 2 indicates that values and effects of the naphtho[2,3-g]phthalazines (**1a–1k**). Compound **1c**, bearing a naphtho[2,3-g]phthalazine showed better activity, with an IC_{50} value of 11.5 μM, compared to kojic acid with an IC_{50} value of 78.0 μM.

Table 2. The compounds (**1a–1k**)—Tyrosinase screening.

Compound	Concentration (μg/mL) [a]			IC_{50} μg/mL (μM)
	25	50	100	
1a	11.02 ± 0.15	22.81 ± 0.19	46.74 ± 0.98	>100
1b	03.05 ± 0.28	17.84 ± 0. 12	36.52 ± 0.98	>100
1c	58.75 ± 0.34	72.84 ± 0. 65	88.52 ± 0.57	06.26 (11.5)
1d	18.75 ± 0.22	37.84 ± 0.43	68.52 ± 0.18	71.46 (142.7)
1e	13.75 ± 0.56	24.84 ± 0.23	55.52 ± 0.06	91.51 (213.6)
1f	20.75 ± 0.66	53.84 ± 0.19	78.52 ± 0.63	56.24 (125.4)
1g	14.75 ± 0.54	31.84 ± 0.13	62.52 ± 0.17	80.68 (155.9)
1h	19.75 ± 0.47	23.84 ± 0.24	43.52 ± 0.05	>100
1i	16.75 ± 0.38	21.84 ± 0.29	40.52 ± 0.29	>100
1j	19.75 ± 0.23	34.84 ± 0.34	54.52 ± 0.88	88.59 (165.7)
1k	21.75 ± 0.17	41.84 ± 0.10	67.52 ± 0.15	69.18 (136.0)
Kojic acid	55.61 ± 0.87	68.10 ± 0.11	84.12 ± 0.18	11.09 (78.0)

[a] Data represent the mean ± standard error of the mean values of three separate experiments.

2.2.2. Inhibitory Mechanism

2-Hydroxyketone is in compound **1a–1k** and kojic acid, and plays a major role in their mechanism. The compound **1c** had the highest inhibition; the mechanism of inhibition is represented in Scheme 4 [26]. The kinetic behavior was studied using compound **1c** at different concentrations with respect to L-DOPA, by mushroom tyrosinase. Figure 6 shows the lineweaver Burk plots, which indicated **1c** is a competitive inhibitor. The result, due to the abscisse 1/[L-DOPA] is the reciprocal of the L-DOPA concentrations and reaction rate of tyrosinase activity.
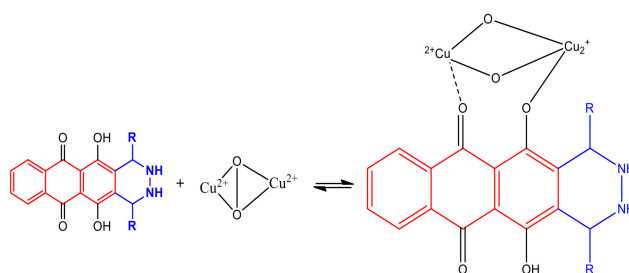
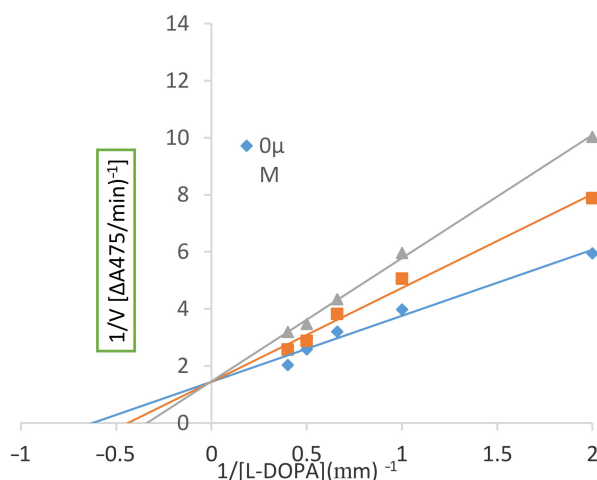**Scheme 4.** Tyrosinase with reversible competitive binding of compound **1c** (binuclear active site).

Figure 6. Inhibition of compound **1c**—Lineweaver–Burk plot.

2.2.3. Molecular Docking

The compound **1c** and control Kojic acid were docked with 2Y9X protein via Schrodinger Suite. The compound **1c** showed a dock score (−5.6 kcal/mol) higher than that of kojic acid, with a dock score of (−5.2 kcal/mol) in 2Y9X protein. The hydrogen bond stretches of compound **1c** and kojic acid were strong hydrogen bonds, and 3.5Å in 2Y9X. The **1c** forms three hydrogen bonds on the 2Y9X protein. The amino acid residues Arg268 (bond length: 5.85), Ser282 (bond length: 4.25), and Val283 (bond length: 3.62) were intricate in the hydrogen bonding interface. Residues of His61, His85, Phe90, His94, Phe192, Trp227, Val248, Gly249, Met257, Asn260, Thr261, His263, Phe264, Leu275, Pro277, Met280, Gly281, Pro284, His285, Ala286, Phe292, and His296 were involved in the hydrophobic interactions. The connections of **1c** with the 2Y9X protein are shown in Figure 7. One hydrogen bond is formed from the control, kojic acid, in the 2Y9X protein receptor. The amino acid residue interaction with hydrogen bonding was involved in His263 (bond length: 1.79). Hydrophobic interactions were involved in the amino acid residues of Met280, Val283 and His296. The 2Y9X protein interactions with the control kojic acid are shown in Figure 8. The results of compound **1c** show the better inhibition than the control kojic acid in mushroom tyrosinase protein 2Y9X. The tyrosinase enzyme inhibition values are listed in Table 3.

Table 3. Molecular docking interactions of compound 1c and control kojic acid against mushroom Table 2. Y9X.

Ligand	Dock Score	H. Bond	Glide E. Model	No of Interactions	Interacting Residues	Bond Length
1c	−5.6	−2.4	−36.865	3	Arg268, Ser282, and Val283	5.85, 4.25, and 3.62
Kojic acid	−5.2	−2.2	−17.030	1	His263	1.79

(**a**) Docked complex   (**b**) molecular surface

(**c**) 3D   (**d**) 2D
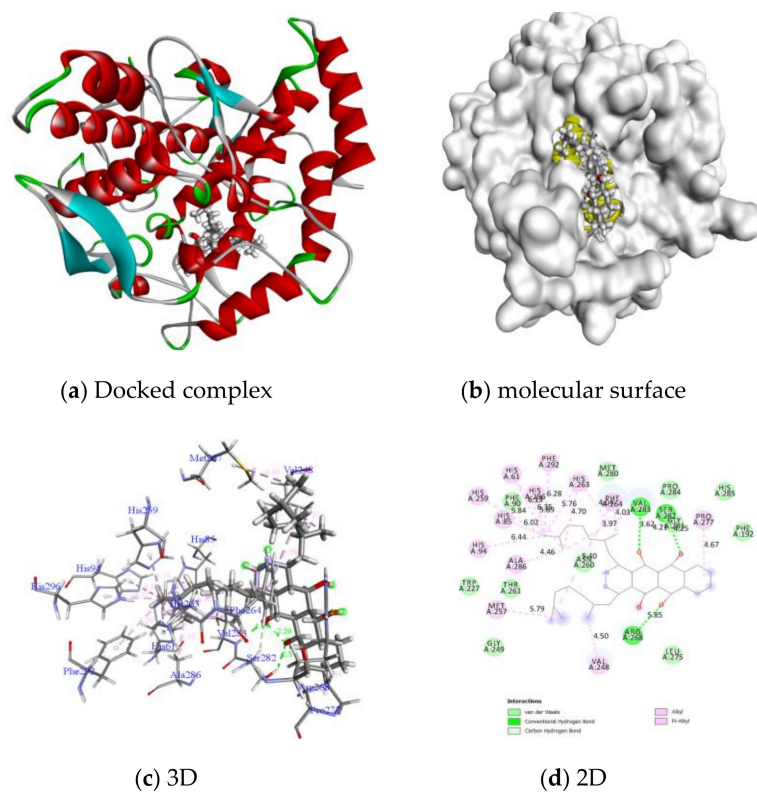
Figure 7. Molecular docking of compound **1c** with binding site of 2Y9X protein.

(**a**) Docked complex   (**b**) molecular surface
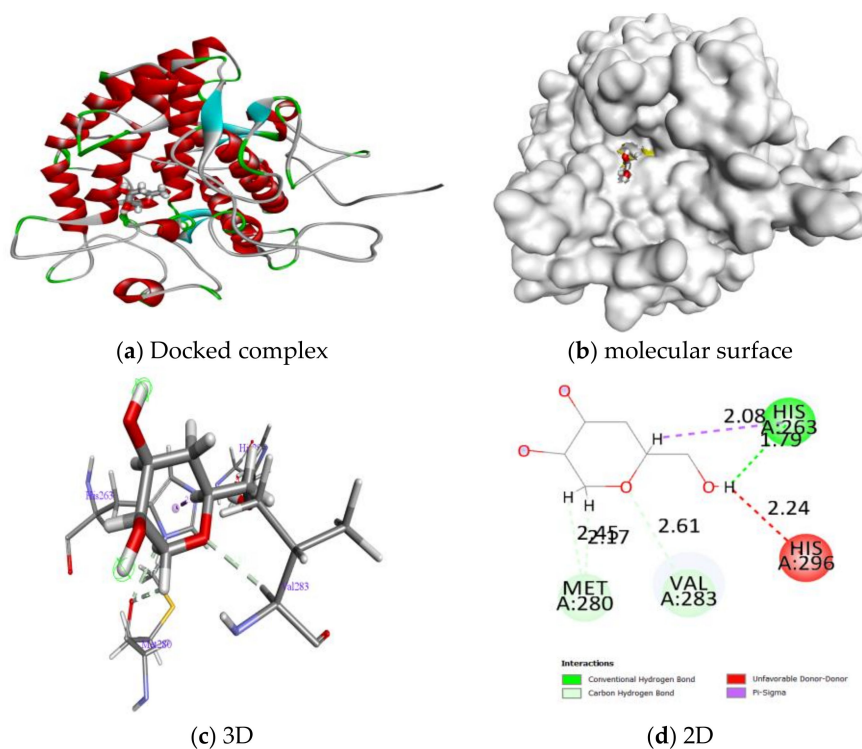

(**c**) 3D   (**d**) 2D

Figure 8. Molecular docking of kojic acid binding site of 2Y9X protein.

2.2.4. Cytotoxicity Activity

The 50% growth inhibition (GI_{50}), tumor growth inhibition (TGI), and lethal concentration 50 (LC_{50}) values were determined. Compound **1c** was highly active against HepG2 cells (GI_{50}:0.01 μM),

MCF-7 (0.03 μM), HeLa (0.04 μM) when compared with doxorubicin and other compounds. All other compounds had moderate active in cytotoxicity screening. The cytotoxic screening results are presented in Table 4.

Table 4. Cytotoxicity activity of compounds (**2a**–**2k**).

Comp. No.	HepG2			MCF-7			HeLa		
	GI$_{50}$ (μM)	TGI (μM)	LC$_{50}$ (μM)	GI$_{50}$ (μM)	TGI (μM)	LC$_{50}$ (μM)	GI$_{50}$ (μM)	TGI (μM)	LC$_{50}$ (μM)
1a	3.60 ± 0.18	8.90 ± 0.74	15.40 ± 0.12	0.71 ± 0.08	14.60 ± 0.70	22.60 ± 0.32	3.50 ± 0.19	07.80 ± 0.16	14.80 ± 0.10
1b	0.05 ± 0.02	0.19 ± 0.05	0.93 ± 0.02	0.15 ± 0.02	0.38 ± 0.34	0.89 ± 0.08	0.21 ± 0.17	0.59 ± 0.10	01.58 ± 0.18
1c	0.01 ± 0.02	0.15 ± 0.31	0.61 ± 0.11	0.03 ± 0.00	0.29 ± 0.41	0.98 ± 0.09	0.04 ± 0.06	0.58 ± 0.19	0.98 ± 0.09
1d	0.16 ± 0.07	0.49 ± 0.28	1.20 ± 0.01	9.80 ± 0.95	18.20 ± 0.74	36.20 ± 0.63	4.30 ± 0.20	09.40 ± 0.12	15.10 ± 0.10
1e	4.70 ± 0.10	10.30 ± 0.24	28.20 ± 0.40	10.0 ± 0.34	20.10 ± 0.64	42.00 ± 0.41	10.10 ± 0.24	21.30 ± 0.14	36.70 ± 1.23
1f	6.20 ± 0.94	13.20 ± 0.10	22.30 ± 0.52	09.5 ± 0.15	15.60 ± 0.24	32.90 ± 0.35	5.70 ± 0.03	19.20 ± 0.19	26.50 ± 0.95
1g	0.13 ± 0.05	0.28 ± 0.12	0.56 ± 0.02	0.48 ± 0.08	0.95 ± 0.04	1.59 ± 0.74	0.06 ± 0.01	0.16 ± 0.06	0.30 ± 0.05
1h	6.10 ± 0.12	12.80 ± 0.13	26.90 ± 0.22	11.60 ± 0.91	26.70 ± 0.28	49.50 ± 0.74	13.30 ± 0.14	29.40 ± 0.18	52.00 ± 0.04
1i	12.30 ± 0.18	26.80 ± 0.25	45.30 ± 0.19	1.28 ± 0.10	2.91 ± 0.32	6.49 ± 0.74	4.10 ± 0.18	09.20 ± 0.06	15.80 ± 0.62
1j	6.30 ± 0.42	13.10 ± 0.65	26.90 ± 0.72	2.80 ± 0.65	4.90 ± 0.34	1.20 ± 0.08	6.10 ± 0.07	13.90 ± 0.10	30.10 ± 0.18
1k	15.50 ± 0.02	30.10 ± 0.31	87.20 ± 0.11	17.10 ± 0.74	26.10 ± 0.41	49.30 ± 0.09	19.60 ± 0.06	31.90 ± 0.19	87.60 ± 0.19
Std.	0.01 ± 0.00	0.13 ± 0.01	0.58 ± 0.02	0.02 ± 0.00	0.21 ± 0.06	0.74 ± 0.09	0.05 ± 0.01	0.41 ± 0.10	0.88 ± 0.05

Value expressed are means ± SD error of the mean values of three separate experiments. Standard: Doxorubicin.

3. Experimental Section

3.1. Synthesis

FT IR (4000–400 cm^{-1}) was recorded ED via Shimadzu 8201pc (Shimadzu, Tokyo, Japan). The ^{1}H and ^{13}C NMR recording was via JEOL-300 Mhz (Jeol, Tokyo, Japan). The elementer analyzer model Varian EL III (Varian, Inc., Karlsruhe, Germany) was used for analysis of elemental presences. Thin-layer chromatography was used for purity checking.

Synthesis of Telmisartan Mediated Copper Nanoparticles (Tel-Cu-NPs)

The mixture of CuCl$_2$· 2H$_2$O (0.5 mmol, 5 mL), and telmisartan (1 mmol, 10 mL) was added to 10 mL of ethanol, then the reaction mixture was given 1 M NaOH with stirring and maintained at pH 7. The reaction mixture converted to a blue precipitate followed by the addition of 15 mL of water. The bile precipitate was obtained, then the precipitate was filtered and purified with suitable techniques.

General Preparation of Compounds (**1a**–**1k**)

To a solution of 1,4-dihydroxy-anthraquinone (16.02 g, 0.10 mol) in EtOH (150 mL), aldehyde (0.30 mol), hydrazine hydrate (2.44 g, 0.02 mol), and catalyst Tel-Cu-NPs (1.0 mg) were mixed in a mortar at RT. Achievement of the product as checked by TLC. The insoluble crude product was filtered, then the final product was separated from the column chromatography using suitable eluting solvent. Similarly, compounds (**1b**–**1k**) were synthesized by using the same method.

Catalyst recovery studies: In order to investigate the reusability of the catalyst, after completion of the reaction, copper nanoparticles were recovered by filtration of the mixture in a vacuum and thoroughly washed with ethylacetate. The final product was soluble in EtOAc solvent and we then separated the final product from the mixture. The copper nano catalyst was thoroughly washed with water, followed by filtering and then drying in an oven at 60 °C, and was then used for the next reaction without any reactivation [27].

Characterization of Target Compounds

5,12-dihydroxy-1,2,3,4-tetrahydronaphtho[2,3-g]phthalazine-6,11-dione (**1a**)

Yellow solid; yield 88%; mw: 296.28; mp: 126–127 °C; IR (KBr, cm^{-1}): 3408, 3282, 2842, 1752, 1684, 804, 745; ^{1}H NMR (DMSO-d$_6$) δ 9.20 (s, 2H), 8.29 (d, *J* = 11.6 Hz, 2H, Ar), 7.88 (2H, dd, *J* = 11.6 Hz, *J* = 11.2 Hz, Ar), 5.31 (s, 2H, OH), 3.91 (4H, s, CH$_2$); ^{13}C NMR (DMSO-d$_6$) δ 187.1 (2C, C=O), 151.9 (2C, C-OH), 133.6, 132.1, 126.8 (6C, Ar), 132.0 (2C), 113.9 (2C), 50.7 (2C, C-N-N); EIMS (*m/z*): 296.30 [M]$^{+}$; Anal. Calcd. For C$_{16}$H$_{12}$N$_2$O$_4$: C, 64.86; H, 4.08; N, 9.46; Found: C, 64.84; H, 4.10; N, 9.46;

5,12-dihydroxy-1,4-di(prop-1-en-1-yl)-1,2,3,4- tetrahydro naphtho[2,3-g]phthalazine-6,11-dione (**1b**)

Yellow solid; yield 85%; mw: 376.41; mp: 130–132 °C; IR (KBr): 3409, 3280, 2843, 1753, 1684, 806, 748 cm^{-1}; ^{1}H NMR (300 MHz) δ 9.23 (s, 2H, NH), 8.27 (d, *J* = 11.4 Hz, 2H, Ar), 7.87 (dd, 2H, *J* = 11.6 Hz, *J* = 11.2 Hz, Ar), 6.08 (s, 2H), 5.41 (s, 2H, CH=C̲H), 5.39 (s, 2H, OH), 4.5 (s, 2H), 2.09 (s, 6H); ^{13}C NMR (DMSO-d$_6$) δ 187.3 (2C), 151.6 (2C, C-OH), 133.6, 132.1, 126.8 (6C, Ar), 127.1 (2C), 126.4 (2C), 126.2 (2C, C=C̲), 113.9 (2C), 60.4 (2C, C-N-N), 17.6 (2C, CH$_3$); EI-MS *m/z*: 376.45 [M]$^+$; Anal. Calcd. For C$_{22}$H$_{20}$N$_2$O$_4$: C, 70.20; H, 5.36; N, 7.44; Found: C, 70.22; H, 5.37; N, 7.43;

1,4-bis(2,6-dimethylhepta-1,5-dien-1-yl)-5,12-dihydroxy-1,2,3,4-tetrahydronaphtho[2,3-g]phthalazine-6,11-dione (**1c**)

Yellow solid, yield 84%; mw: 540.69; mp: 141–142 °C; IR (KBr): 3406, 3282, 2845, 1754, 1682, 804, 746 cm^{-1}; ^{1}H NMR (300 MHz) δ 9.84 (s, 2H, NH), 8.26 (d, *J* = 11.2 Hz, 2H, Ar), 7.87 (dd, 2H, *J* = 11.4 Hz, *J* = 11.2 Hz, Ar), 5.80 (s, 2H, C̲H=C), 5.31 (s, 2H, OH), 5.20 (s, 2H, CH=C), 4.50 (s, 2H, CH), 2.0 (s, 8H, CH$_2$), 1.82 (s, 12H, CH$_3$), 1.70 (s, 6H); ^{13}C NMR (75 MHz) δ 187.4 (2C), 151.5 (2C, C-OH), 135.7 (2C), 132.2 (2C), 133.6, 132.1, 126.8 (6C, Ar), 126.6 (2C), 123.5 (2C, C̲=C), 54.2 (2C, C-N-N), 113.9 (2C), 116.7 (2C, C̲=C), 39.7, 26.4 (4C, CH$_2$), 24.6, 18.6, 16.4 (6C, CH$_3$); EIMS (*m/z*) 540.72 [M]$^+$; Anal. Calcd. For C$_{34}$H$_{40}$N$_2$O$_4$: C, 75.53; H, 7.46; N, 5.18; Found: C, 75.50; H, 7.48; N, 5.17;

5,12-dihydroxy-1,4-di(styryl)-1,2,3,4-tetrahydronaphtho[2,3-g]phthalazine-6,11-dione (**1d**)

Yellow solid, yield 83%; mw: 500.54; mp: 152–153 °C; IR (KBr, cm^{-1}): 3408, 3280, 2843, 1751, 1683, 803, 742; ^{1}H NMR (DMSO-d$_6$) δ 9.89 (s, 2H, NH), 8.26 (d, *J* = 11.0 Hz, 2H, Ar), 7.86 (dd, *J* = 11.1 Hz, *J* = 11.2 Hz, 2H, Ar), 7.24–7.40 (m, *J* = 11.6 Hz, 10H, Ph), 6.65 (s, 2H), 6.37 (s, 2H, CH=C̲H), 5.31(s, 2H, OH), 4.51 (2H, s, CH); ^{13}C NMR (75 MHz, δ: 187.1 (2C), 151.9 (2C, C-OH), 126.6 (2C), 113.9 (2C), 129.0 (2C, C=C), 136.4, 128.6, 128.5, 127.9 (12C, Ph), 126.8, 132.8, 133.6 (6C, Ar), 123.3 (2C), 60.3 (2C, C-N-N); EIMS (*m/z*):500.58 [M]$^+$; Anal. Calcd. For C$_{32}$H$_{24}$N$_2$O$_4$: C, 76.78; H, 4.83; N, 5.60; Found: C, 76.80; H, 4.80; N, 5.62

1,4-di(furan-2-yl)-5,12-dihydroxy-1,2,3,4-tetrahydronaphtho[2,3-g]phthalazine-6,11-dione (**1e**)

Yellow solid, yield 85%; mw: 428.39; mp: 150–151 °C; IR (KBr, cm^{-1}): 3410, 3284, 2840, 1752, 1684, 805, 740; ^{1}H NMR (DMSO-d$_6$) δ 9.86 (s, 2H, NH), 8.26 (d, *J* = 11.8 Hz, 2H, Ar), 7.86 (2H, dd, *J* = 11.9 Hz, J = 11.2 Hz, Ar), 7.65 (d, 2H, *J* = 7.8 Hz, Furyl), 6.44 (dd, *J* = 7.8 Hz, *J* = 7.6 Hz, 2H, Furyl), 6.26 (d, 2H, J=, Furyl), 5.42 (s, 2H, CH), 5.30 (s, 2H, OH); ^{13}C NMR (75 MHz) δ 187.2 (2C), 152.5, 106.7, 110.6, 142.1 (8C, Furyl), 151.6 (2C, C-OH), 133.6, 132.1, 126.8 (6C, Ar), 133.0 (2C), 113.9 (2C), 61.4 (2C, C-N-N); EIMS (*m/z*): 428.43 [M]$^+$; Anal. Calcd. For C$_{24}$H$_{16}$N$_2$O$_6$: C, 67.29; H, 3.76; N, 6.54; Found: C, 67.30; H, 3.75; N, 6.55;

5,12-dihydroxy-1,4-diphenyl-1,2,3,4-tetrahydronaphtho[2,3-g]phthalazine-6,11-dione (**1f**)

Yellow solid, yield 82%; mw: 448.47; mp: 162–164 °C; IR (KBr, cm^{-1}): 3412, 3286, 2842, 1754, 1686, 807, 742; ^{1}H NMR (DMSO-d$_6$) δ 9.89 (s, 2H, NH), 8.22 (d, *J* = 11.8 Hz, 2H, Ar), 7.86 (dd, 2H, *J* = 11.7 Hz, J = 11.6 Hz, Ar), 7.37 (d, 4H, *J* = 9.8 Hz, Ph), 7.33 (dd, 4H, *J* = 9.8 Hz, *J* = 9.2 Hz, Ph), 7.26 (dd, 2H, *J* = 9.8 Hz, *J* = 9.2 Hz, Ph), 5.29 (s, 2H, OH), 5.11 (2H, s, CH); ^{13}C NMR (DMSO-d$_6$) δ 187.6 (2C), 153.9 (2C, C-OH), 142.7, 128.2, 129.2, 126.2 (12C, Ph), 134.9 (2C), 133.6, 132.1, 126.8 (6C, Ar), 114.1 (2C), 60.8 (2C, C-N-N); EIMS(*m/z*): 448.50 [M]$^+$; Anal. Calcd. For C$_{28}$H$_{20}$N$_2$O$_4$: C, 74.99; H, 4.50; N, 6.25; Found: C, 75.01; H, 4.48; N, 6.26;

1,4-bis(4-chlorophenyl)-5,12-dihydroxy-1,2,3,4-tetrahydronaphtho[2,3-g]phthalazine-6,11-dione (**1g**)

Yellow solid, yield 84%; mw: 517.36; mp: 138–139 °C; IR (KBr, cm^{-1}): 3413, 3285, 2840, 1752, 1684, 805, 740; ^{1}H NMR (DMSO-d$_6$) δ 9.80 (s, 2H, NH), 8.25 (d, *J* = 11.7 Hz, 2H, Ar), 7.84 (2H, dd, *J* = 11.6 Hz, *J* = 11.2 Hz, 2H, Ar), 7.37 (d, *J* = 9.8 Hz, 4H, Ph), 7.17 (d, *J* = 9.8 Hz, *J* = 9.2 Hz, 4H, Ph), 5.32 (s, 2H, OH), 5.19 (s, 2H, CH); ^{13}C NMR (DMSO-*d$_6$*) δ: 187.1 (2C, C=O), 153.9 (2C, C-OH),

140.8, 131.8, 129.6, 129.3 (12C, Ph), 134.9 (2C), 133.6, 132.1, 126.8 (6C, Ar), 114.1 (2C), 60.6 (2C, C-N-N); EIMS (*m/z*): 517.40 [M]$^+$; Anal. Calcd. For $C_{28}H_{18}Cl_2N_2O_4$: C, 65.00; H, 3.51; N, 5.41; Found: C, 65.02; H, 3.53; N, 5.40;

5,12-dihydroxy-1,4-bis(4-hydroxyphenyl)-1,2,3,4-tetrahydronaphtho[2,3-g]phthalazine-6,11-dione (**1h**)

Yellow solid, yield 86%; mw: 480.47; mp: 158–159 °C; IR (KBr, cm^{-1}): 3412, 3284, 2842, 1750, 1682, 804, 742; ^{1}H NMR (DMSO-d$_6$) δ 9.80 (s, 2H, NH), 8.29 (d, *J* = 11.4 Hz, 2H, Ar), 7.85 (dd, *J* = 11.4 Hz, *J* = 11.2 Hz, 2H, Ar), 7.37 (d, *J* = 9.8 Hz, 4H, Ph), 7.17 (d, *J* = 9.8 Hz, 4H, Ph), 5.38(s, 4H, OH), 5.19 (s, 2H, CH); ^{13}C NMR (DMSO-*d$_6$*) δ 187.4 (2C), 153.2 (2C, C-OH), 156.0, 135.3, 116.4, 129.6, (12C, Ph), 134.9 (2C), 114.1 (2C), 133.6, 132.1, 126.8 (6C, Ar), 60.8 (2C, C-N-N); EIMS (*m/z*) 480.50 [M]$^+$; Anal. Calcd. For $C_{28}H_{20}N_2O_6$: C, 69.99; H, 4.20; N, 5.83; Found: C, 69.97; H, 4.23; N, 5.85;

5,12-dihydroxy-1,4-bis(3-nitrophenyl)-1,2,3,4-tetrahydronaphtho[2,3-g]phthalazine-6,11-dione (**1i**)

Yellow solid, yield 85%; mw: 538.46; mp: 165–166 °C; IR (KBr, cm^{-1}): 3410, 3280, 2840, 1752, 1680, 802,740; ^{1}H NMR (DMSO-d$_6$) δ 9.76 (s, 2H, NH), 8.26 (d, *J* = 11.7 Hz, 2H, Ar), 7.86 (d, *J* = 9.8 Hz, 2H, Ph), 8.15 (s, 2H, Ph), 8.07 (d, *J* = 9.8 Hz, 2H, Ph), 7.76 (d, *J* = 9.8 Hz, 2H, Ph), 7.50 (dd, 2H, *J* = 9.8 Hz, *J* = 9.2 Hz, Ph), 5.36 (s, 2H, OH), 5.19 (s, 2H, CH); ^{13}C NMR (DMSO-d$_6$) δ 187.2 (2C), 153.5 (2C, C-OH), 143.6, 124.6, 148.4, 121.4, 130.1, 134.3 (12C, Ph), 134.9 (2C), 133.6, 132.1, 126.8 (6C, Ar), 114.1 (2C), 60.2 (2C, C-N-N); EIMS (*m/z*) 538.48 [M]$^+$; Anal. Calcd. For $C_{28}H_{18}N_4O_8$: C, 62.46; H, 3.37; N, 10.40; Found: C, 62.47; H, 3.35; N, 10.38;

1,4-bis(4-(dimethylamino)phenyl)-5,12-dihydroxy-1,2,3,4-tetrahydronaphtho[2,3-g]phthalazine-6,11-dione (**1j**)

Yellow solid, yield 88%; mw: 534.61; mp: 169–171 °C; IR (KBr) 3412, 3282, 2842, 1754, 1682, 804, 742 cm^{-1}; ^{1}H NMR (300 MHz) δ 9.78 (s, 2H, NH), 8.25 (d, *J* = 11.7 Hz, 2H, Ar), 7.86 (dd, 2H, *J* = 11.6 Hz, *J* = 11.2 Hz, Ar), 7.05 (d, *J* = 9.8 Hz, 4H, Ph), 6.60 (d, *J* = 9.8 Hz, 4H, Ph), 5.32 (s, 2H, OH), 5.19 (s, 2H), 3.01 (s, 12H, N(CH$_3$)$_2$); ^{13}C NMR (75 MHz) δ 187.1 (2C), 153.9 (2C, C-OH), 148.6, 132.2, 113.4, 129.1 (12C, Ph), 134.9 (2C), 133.6, 132.1, 126.8 (6C, Ar), 114.1 (2C), 60.8 (2C, C-N-N), 41.3 (4C, N(CH$_3$)$_2$); EIMS (*m/z*) 534.65 [M]$^+$; Anal. Calcd. For $C_{32}H_{30}N_4O_4$: C, 71.89; H, 5.66; N, 10.48; Found: C, 71.90; H, 5.68; N, 10.46; S, 8.96;

5,12-dihydroxy-1,4-bis(4-methoxyphenyl)-1,2,3,4-tetrahydronaphtho[2,3-g]phthalazine-6,11-dione (**1k**)

Yellow solid, yield 82%; mw: 508.52; mp: 137–139 °C; IR (KBr, cm^{-1}): 3414, 3284, 2840, 1752, 1684, 802, 740; ^{1}H NMR (300 MHz) δ 9.86 (s, 2H, NH), 8.24 (d, *J* = 11.6 Hz, 2H, Ar), 7.89 (2H, dd, *J* = 11.6 Hz, *J* = 11.2 Hz, 2H, Ar), 7.12 (d, *J* = 9.8 Hz, 4H, Ph), 6.87 (d, *J* = 9.8 Hz, 4H, Ph), 5.31 (s, 2H, OH), 5.19 (s, 2H, CH), 3.77 (s, 6H, OCH$_3$); ^{13}C NMR (75 MHz) δ 187.4 (2C), 158.1, 135.0, 114.8, 129.2 (12C, Ph), 153.6 (2C, C-OH), 134.9 (2C), 133.6, 132.1, 126.8 (6C, Ar), 114.1 (2C), (6C, Ar), 114.1 (2C), 60.8 (2C, C-N-N), 41.3 (4C, OCH$_3$); EIMS (*m/z*) 508.54 [M]$^+$; Anal. Calcd. For $C_{30}H_{24}N_2O_6$: C, 70.86; H, 4.76; N, 5.51; Found: C, 70.85; H, 4.77; N, 5.53;

3.2. Biological Activity

3.2.1. Anti-Tyrosinase Activity

The mushroom tyrosinase (powder, ≥1000 unit/mg solid, EC 1.14.18.1) inhibitory activities were measured spectrophotometrically, as defined previously with some modifications [28]. For preparation of the test solution, 12.428 U of mushroom tyrosinase was added to L-DOPA 1.5 mM and 0.1 mM sodium phosphate buffer (pH 6.5), and incubated at 30 °C for 2 min. A total of 3.0 mL of test sample was monitored at 475 nm by a Perkin Elmer Lambda 35 Spectrophotometer (Perkin Elmer Corp, Waltham,

MA, USA). Standard kojic acid was used in this screening, and 50% inhibition (IC_{50}) was calculated and analyzed in three independent experiments.

$$\text{Tyrosinase inhibitory activity (\%)} = [(A - B) - (C - D)] / (A - B) \times 100$$

where A = absorbance of incubation (after) of the blank solution; B = absorbance incubation (before) of the blank solution; C = absorbance of incubation (after) the blank solution; D = absorbance of incubation (before) the blank solution.

3.2.2. Molecular Docking

Agaricus bisporus-mushroom tyrosinase (PDBID: 2Y9X) was downloaded from http://www.rcsb.org [29,30].

Grid Generation and Molecular Docking

The tyrosinase structure was arranged via "Protein Preparation Wizard" by the Maestro interface in the Schrodinger Suite. Originally, bond orders were allotted and the target protein was added. Later, the protein was minimized to attain the congregated RMSD-root mean square deviation of 0.30Å via the OPLS_2005 force field. The active position (binding pocket) of the target protein was demarcated by literature survey and the Protein Data Bank [31–33]. Compound **3c** and control kojic acid were drawn by using 2D sketcher in the Schrodinger Suite for docking studies. The studies were achieved by the target protein with a Glide docking procedure to forecast the conformational positions and docking scores (binding energies) of the ligands inside the active area of the protein. All over the docking mock-ups, both partial and suppleness of the active site remains was achieved by Glide/SP/XP and induced fit docking (IFD) methods. The inhibitor devouring minimum binding energy value that was best scoring, and the outcomes, were examined via the Discovery Studio 2019 software package.

3.2.3. Cytotoxic Activity

The compounds (**1a–1k**) were evaluated for cytotoxic activity using the method in our literature report [34]. The details of the experiment are presented in the Supplementary Materials. The cytotoxic values were confirmed based on at least three independent evaluations.

4. Conclusions

Naphtho[2,3-g]phthalazine (**1a–1k**) Mannich base derivatives were synthesized via the grindstone method using the Tel-Cu-NPs catalyst. We synthesized eleven naphtho[2,3-g]phthalazine derivatives (**1a–1k**) and evaluated their anti-tyrosinase activity. Compound **1c** significantly inhibited tyrosinase (IC_{50} = 11.5 μg/mL). Based on molecular docking, compound **1c** had a good dock score (−5.6 kcal/mol) compared to kojic acid (−5.2 kcal/mol) in 2Y9X protein. Cytotoxicity was screened for in all compounds; **1c** was highly active (GI_{50} = 0.01, 0.03, and 0.04 μM) against HepG2 (liver), MCF-7 (breast), and HeLa (cervical) cancer cell lines, compared to doxorubicin and other compounds. Therefore, these results suggest that naphtho[2,3-g]phthalazine derivatives could serve as a new class of anti-tyrosinase agents.

Conflicts of Interest: The authors declare no conflict of interest.

References

1.　Toda, F.; Tanaka, K.; Sekikawa, A. Host–guest complex formation by a solid–solid reaction. *J. Chem. Soc. Chem. Commun.* **1987**, *4*, 279. [CrossRef]

2.　Mannich, C. Eine Synthese von β-ketonbasen. *Arch. Pharm.* **1917**, *255*, 261–276. [CrossRef]

3.　Manabe, K.; Kobayashi, S. Mannich-Type Reactions of Aldehydes, Amines, and Ketones in a Colloidal Dispersion System Created by a Brønsted Acid−Surfactant-Combined Catalyst in Water. *Org. Lett.* **1999**, *1*, 1965–1967. [CrossRef]

4.　Jing-Bo, Y.; Gang, P.; Zhi-Jiang, J.; Zi-Kun, H.; Wei-Ke, S. Mechanochemical Oxidative Mannich Reaction: Evaluation of Chemical and Mechanical Parameters for the Mild and Chemoselective Coupling of *N-tert*-butoxycarbonyltetrahydroquinolines and Ketones. *Eur. J. Org. Chem.* **2016**, *32*, 5340–5344.

5.　Khanna, G.; Aggarwal, K.; Khuran, J.L. An efficient and confluent approach for the synthesis of novel 3,4-dihydro-2*H*-naphtho[2,3-*e*][1,3]oxazine-5,10-dione derivatives by a three component reaction in ionic liquid. *RSC Adv.* **2015**, *5*, 46448–46454. [CrossRef]

6.　Ghomi, J.S.; Zahedi, S. Novel ionic liquid supported on Fe_3O_4 nanoparticles and its application as a catalyst in Mannich reaction under ultrasonic irradiation. *Ultrason Sonochem* **2017**, *34*, 916–923. [CrossRef]

7.　Ling-Ling, W.; Yang, X.; Da-Cheng, Y.; Zhi, G.; Yan-Hong, H. Biocatalytic asymmetric Mannich reaction of ketimines using wheat germ lipase, Catal. *Sci. Technol.* **2016**, *6*, 3963–3970.

8.　Mostafa, A.A.F.; SathishKumar, C.; Al-Askar, A.M.; Sayed, S.R.; SurendraKumar, R.; Idhayadhulla, A. Synthesis of novel benzopyran-connected pyrimidine and pyrazole derivatives via a green method using Cu(II)-tyrosinase enzyme catalyst as potential larvicidal, antifeedant activities. *RSC Adv.* **2019**, *9*, 25533–25543. [CrossRef]

9.　Whitaker, J.R. Polyphenol Oxidase. In *Food Enzymes*; Springer: Boston, MA, USA, 1995. [CrossRef]

10.　Fenoll, L.G.; Penalver, M.J.; RodríguezLopez, J.N.; Varon, R.; GarcíaCanovas, F.; Tudela, J. Tyrosinase kinetics: Discrimination between two models to explain the oxidation mechanism of monophenol and diphenol substrates. *Int. J. Biochem. Cell. Biol.* **2004**, *36*, 235–246. [CrossRef]

11.　Costin, G.E.; Hearing, V.J. Human skin pigmentation: Melanocytes modulate skin color in response to stress. *FASEB J.* **2007**, *21*, 976–994. [CrossRef]

12.　Vashi, N.A.; Kundu, R.V. Facial hyperpigmentation: Causes and treatment. *Br. J. Dermatol.* **2013**, *169*, 41–56. [CrossRef] [PubMed]

13.　Hasegawa, T. Tyrosinase-Expressing Neuronal Cell Line as in vitro Model of Parkinson's disease. *Int. J. Mol. Sci.* **2010**, *11*, 1082–1089. [CrossRef] [PubMed]

14.　Van Gorkom, B.A.; De Vries, E.G.; Karrenbeld, A.; Leibeuker, J.H. Review article: Anthranoid laxatives and their potential carcinogenic effects, Aliment. *Pharmacol. Ther.* **1999**, *13*, 443–452. [CrossRef] [PubMed]

15.　Shrestha, J.P.; Fosso, M.Y.; Bearss, J.; Chang, C.W.T. Synthesis and anticancer structure activity relationship investigation of cationic anthraquinone analogs. *Eur. J. Med. Chem.* **2014**, *77*, 96–102. [CrossRef]

16.　Khan, N.; Karodi, R.; Siddiqui, A.; Thube, S.; Rub, R. Development of anti-acne gel formulation of anthraquinones rich fraction from *Rubia cordifolia* (Rubiaceae). *Int. J. Appl. Res. Nat. Prod.* **2011**, *4*, 28–36.

17.　Davis, R.; Agnew, P.; Shapiro, E. Antiarthritic activity of anthraquinones found in aloe for podiatric medicine. *J. Am. Podiatr. Med. Assoc.* **1986**, *76*, 61–66. [CrossRef]

18.　Wuthi-udomlert, M.; Kupittayanant, P.; Gritsanapan, W. In vitro evaluation of antifungal activity of anthraquinone derivatives of *Senna alata*. *J. Health Res.* **2010**, *24*, 117–122.

19.　Fosso, M.Y.; Chan, K.Y.; Gregory, R.; Chang, C.W.T. Library Synthesis and Antibacterial Investigation of Cationic Anthraquinone Analogs. *ACS Comb. Sci.* **2012**, *14*, 231–235. [CrossRef]

20.　Barnard, D.L.; Fairbairn, D.W.; O'Neill, K.L.; Gage, T.L.; Sidwell, R.W. Anti-human cytomegalovirus activity and toxicity of sulfonated anthraquinones and anthraquinone derivatives. *Antiviral. Res.* **1995**, *28*, 317–329. [CrossRef]

21.　Seo, E.J.; Ngoc, T.M.; Lee, S.M.; Kim, Y.S.; Jung, Y.S. Chrysophanol-8-*O*-glucoside, an Anthraquinone Derivative in Rhubarb, Has Antiplatelet and Anticoagulant Activities. *J. Pharmacol. Sci.* **2012**, *118*, 245–254. [CrossRef]

22. Jackson, T.C.; Verrier, J.D.; Kochanek, P.M. Anthraquinone-2-sulfonic acid (AQ2S) is a novel neurotherapeutic agent. *Cell Death Dis.* **2013**, *4*, 451. [CrossRef] [PubMed]

23. Bhasin, A.K.; Chauhan, P.; Chaudhary, S. A novel sulfur-incorporated naphthoquinone as a selective "turn-on" fluorescence chemical sensor for rapid detection of Ba^{2+} ion in semi-aqueous medium. *Sens. Actuators B Chemical.* **2019**, *294*, 116–122. [CrossRef]

24. Kumar, P.; Ghosh, A.; Jose, D.A. A simple colorimetric sensor for the detection of moisture in organic solvents and building materials: Applications in rewritable paper and fingerprint imaging. *Analyst* **2019**, *144*, 594–601. [CrossRef] [PubMed]

25. Rodríguez-Ciria, M.; Sanz, A.M.; Yunta, M.J.R.; Gómez-Contreras, F.; Navarro, P.; Sánchez-Moreno, M.; Boutaleb-Charki, S.; Osuna, A.; Castiñeiras, A.; Pardo, M.; et al. 1,4-Bis (alkyla mino) benzo[*g*]phthalazines able to form dinuclear complexes of Cu(II) which as free ligands behave as SOD inhibitors and show efficient in vitro activity against *Trypanosoma cruzi*. *Bioorg. Med. Chem.* **2007**, *15*, 2081–2091.

26. Battaini, G.; Monzani, E.; Casella, L.; Santagostini, L.; Pagliarin, R. Inhibition of the catecholase activity of biomimetic dinuclear copper complexes by kojic acid. *J. Biol. Inorg. Chem.* **2000**, *5*, 262–268. [CrossRef]

27. Naeimi, H.; Brojerdi, S.S. Facile and Efficient One-Pot Synthesis of Anthraquinones from Benzene Derivatives Catalyzed by Silica Sulfuric Acid. *Polycycl. Aromat. Compd.* **2014**, *34*, 504–517. [CrossRef]

28. Xia, L.L.; Idhayadhulla, A.; Lee, Y.R.; Wee, Y.J.; Kim, S.H. Anti-tyrosinase, antioxidant, and antibacterial activities of novel 5-hydroxy-4-acetyl-2,3-dihydronaphtho[1,2-b]furans. *Eur. J. Med. Chem.* **2014**, *86*, 605–612.

29. Friesner, R.A.; Murphy, R.B.; Repasky, M.P.; Frye, L.L.; Greenwood, J.R.; Halgren, T.A.; Sanschagrin, P.C.; Mainz, D.T. Extra Precision Glide: Docking and Scoring Incorporating a Model of Hydrophobic Enclosure for Protein−Ligand Complexes. *J. Med. Chem.* **2006**, *49*, 6177–6196. [CrossRef]

30. Farid, R.; Day, T.; Friesner, R.A.; Pearlstein, R.A. New insights about HERG blockade obtained from protein modeling, potential energy mapping, and docking studies. *Bioorg. Med. Chem.* **2006**, *14*, 3160–3173. [CrossRef]

31. Saeed, A.; Mahesar, P.A.; Channar, P.A.; Abbas, Q.; Larik, F.A.; Hassan, M.; Raza, H.; Seo, S.Y. Synthesis, molecular docking studies of coumarinyl-pyrazolinyl substituted thiazoles as non-competitive inhibitors of mushroom tyrosinase. *Bioorg. Chem.* **2017**, *74*, 187–196.

32. Larik, F.A.; Saeed, A.; Channar, P.A.; Muqadar, U.; Abbas, Q.; Hassan, M.; Seo, S.Y.; Bolte, M. Design, synthesis, kinetic mechanism and molecular docking studies of novel 1-pentanoyl-3-arylthioureas as inhibitors of mushroom tyrosinase and free radical scavengers. *Eur. J. Med. Chem.* **2017**, *141*, 273–281. [CrossRef] [PubMed]

33. Hassan, M.; Ashraf, Z.; Abbas, Q.; Raza, H.; Seo, S.Y. Exploration of Novel Human Tyrosinase Inhibitors by Molecular Modeling, Docking and Simulation Studies. *Interdiscip. Sci.* **2018**, *10*, 68–80. [CrossRef] [PubMed]

34. Kumar, R.S.; Moydeen, M.; Al-Deyab, S.S.; Aseer, M.; Idhayadhulla, A. Synthesis of new morpholine -connected pyrazolidine derivatives and their antimicrobial, antioxidant, and cytotoxic activities. *Bioorg. Med. Chem. Lett.* **2017**, *27*, 66–71. [CrossRef] [PubMed]